THE JOURNAL OF PHYSICAL CHEMISTRY LETTERS
A JOURNAL OF THE AMERICAN CHEMICAL SOCIETY

pubs.acs.org/JPCL

Letter

Targeting Individual Tautomers in Equilibrium by Resonant Inelastic X-ray Scattering

Vinícius Vaz da Cruz,* Robby Büchner, Mattis Fondell, Annette Pietzsch, Sebastian Eckert, and Alexander Föhlisch

Cite This: *J. Phys. Chem. Lett.* 2022, 13, 2459−2466

Read Online

ACCESS | Metrics & More | Article Recommendations | Supporting Information

ABSTRACT: Tautomerism is one of the most important forms of isomerism, owing to the facile interconversion between species and the large differences in chemical properties introduced by the proton transfer connecting the tautomers. Spectroscopic techniques are often used for the characterization of tautomers. In this context, separating the overlapping spectral response of coexisting tautomers is a long-standing challenge in chemistry. Here, we demonstrate that by using resonant inelastic X-ray scattering tuned to the core excited states at the site of proton exchange between tautomers one is able to experimentally disentangle the manifold of valence excited states of each tautomer in a mixture. The technique is applied to the prototypical keto−enol equilibrium of 3-hydroxypyridine in aqueous solution. We detect transitions from the occupied orbitals into the LUMO for each tautomer in solution, which report on intrinsic and hydrogen-bond-induced orbital polarization within the π and σ manifolds at the proton-transfer site.

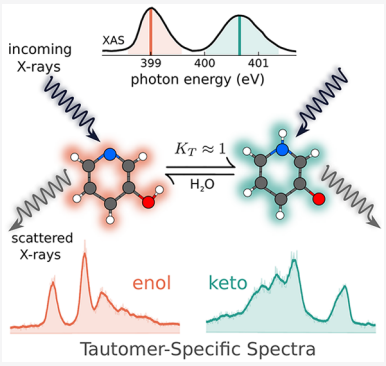

Tautomerism constitutes a form of isomerization involving species that readily interconvert. The most prevalent manifestation of tautomerism is caused by a change in the position of a proton within a molecule, denoted prototropic tautomerism. Although a seemingly subtle change, it imparts decisive modifications in chemical bonding and polarity, consequently defining molecular properties and functionality. Tautomerization plays decisive roles in many chemical processes, such as determining the mechanisms of chemical reactions.[1] Its biological importance is reflected in the tautomerism of amino acids[2,3] that affects the folding of proteins[4] as well as their pocket-binding properties.[5]

Molecules exhibiting tautomerism readily interconvert, coexisting at a ratio dictated by the tautomeric constant K_T, which depends on a number of parameters, e.g., environment polarity and intra- and intermolecular hydrogen bonding. Apt manipulation of these chemical parameters enables biasing the equilibrium in favor of a given tautomer and hence learning about the properties of each individual species. However, tautomers can also be inseparable or can exist only as short-lived intermediates, which preclude isolation and a detailed investigation of their properties.

Accessing the electronic structure of individual tautomers in equilibrium has been a long-standing challenge in chemical spectroscopy. Considering traditional UV−vis absorption spectroscopy, one is often faced with the problem that the lowest $\pi \rightarrow \pi^*$ absorption bands of individual tautomers overlap strongly, meaning that obtaining their individual spectra experimentally is unfeasible as a rule. In this context, the equilibrium has to be perturbed by creating solvent mixtures or manipulating the pH so as to detect variations in the spectra, which in turn need to be decomposed by assuming band shapes and using statistical methods.[6,7]

Here, we propose resonant inelastic X-ray scattering[8] (RIXS) as an elegant solution to this problem. In the RIXS process, the valence electronic excited states of a molecule are reached indirectly, following decay from a resonantly excited intermediate state, in close analogy to resonant Raman spectroscopy. In RIXS, however, the intermediate states are core excited states which are element-specific and highly sensitive to the local chemical environment of individual atoms in a molecule. These attributes have led to insight into the bonding in transition-metal complexes,[9] proton-transfer dynamics in organics,[10] and hydrogen bonding in liquid water.[11]

We demonstrate the unique capability of RIXS to investigate tautomeric equilibria using the prototypical keto−enol equilibrium of 3-hydroxypyridine (3HP) as a show case. In aqueous solution, 3HP exists as a 1:1 mixture of the enol form and the zwitterionic keto form (K_T = 1.17[12]). Using RIXS, we are able to disentangle the excited-state manifold of each individual tautomer, detecting excited states into the XUV region associated with deep-lying bonding orbitals which shed

Received: October 21, 2021
Accepted: February 1, 2022
Published: March 10, 2022

light on the bonding differences between the species as well as on the interactions with the solvent, and address the origin of tautomerism at the molecular orbital level.

In Figure 1a, the keto−enol equilibrium of 3HP is displayed. Although in the gas phase the enolic form is greatly favored, in aqueous solution the zwitterionic keto form is highly stabilized by hydrogen bonds[13−15] to the point where both structures coexist in nearly equal proportions.[12] Figure 1b displays the UV−vis absorption spectrum of the 3HP tautomeric mixture. It can be clearly seen that we have strong overlap between the bands of each species. Underneath the experimental spectra, we display a decomposition of the spectrum into components, as proposed in the seminal work of Metzler and Snell.[12]

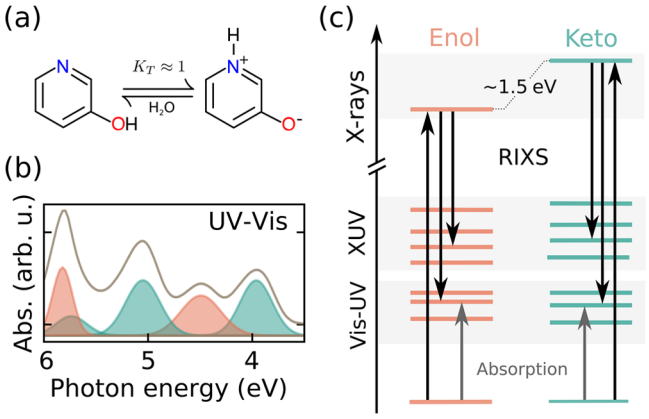

Figure 1. Tautomeric equilibrium in 3-hydroxypyridine and the overlapping spectral response problem. (a) Chemical structure of the species involved in the tautomeric equilibrium of 3-hydroxypyridine (3HP) in aqueous solution (K_T = 1.17[12]). (b) UV−vis absorption spectrum of aqueous 3HP (solid line) and the respective band decomposition scheme[12] shown by shaded areas for the keto (green) and enol (red) forms. (c) Diagram of electronic transitions underlying the UV−vis absorption and RIXS spectra of 3HP. While the $\pi \rightarrow \pi^*$ levels energetically overlap, the $1s_N \rightarrow \pi^*$ levels are shifted by about 1.5 eV, allowing the species to separate through resonant excitation.

This decomposition relied on the comparison of the spectra in different solvents, allowing the assignment of the first and third peaks to the keto form and the second peak to the enol form. Although the analysis of the lowest absorption bands allowed for the determination of the equilibrium constant, it provides only limited information on the full electronic structure of the individual tautomeric species. Moreover, the energy range of a typical UV−vis spectrum is limited both by experimental constraints and by the strong solvent absorption background for higher photon energies.

The limitations outlined above may be overcome by utilizing the core excited states of the system. We shall focus on the N K-edge, specifically, on excitations from the N 1s orbital into the LUMO π^* orbital. Such highly excited states, with a hole localized on the nitrogen atom, show a high sensitivity to the chemical environment. Hence, the presence or absence of a proton bound to the nitrogen atom introduces a large chemical shift between the core excited states of the tautomers.[15] Indeed, the literature abounds with examples discussing the protonation shift of X-ray absorption resonances between species in solution.[10,15−18]

Figure 1c shows how we use RIXS to exploit the chemical shift of the π^* resonance upon proton transfer between tautomers to yield an experimentally pure spectrum for each species. As shown in the diagram, by tuning the X-ray excitation to each of the well-separated core excited resonances we can detect the emitted photons upon decay to the manifold of final states, which in turn are states with valence excitation character. In this specific case, the RIXS spectrum of each tautomer will contain transitions from the occupied orbital manifold into the LUMO, provided the states have significant N 2p character. Thus, we can also observe the electronic changes in the bonding orbitals of the system and are not limited to only the frontier orbitals. Therefore, we expect to map the local electronic structure of each tautomer at the nitrogen atom, which is one of the proton-transfer sites in the heterocycle.

The basic experimental framework is depicted in Figure 2a. The tautomeric mixture in a liquid jet is exposed to an X-ray beam with a narrow energy bandwidth as well as a well-defined polarization vector. The intensity and energy of the respective scattered photons are subsequently detected. Scanning the incident photon energy across the π^* resonances of each tautomer leads to the two-dimensional map presented in Figure 2b.

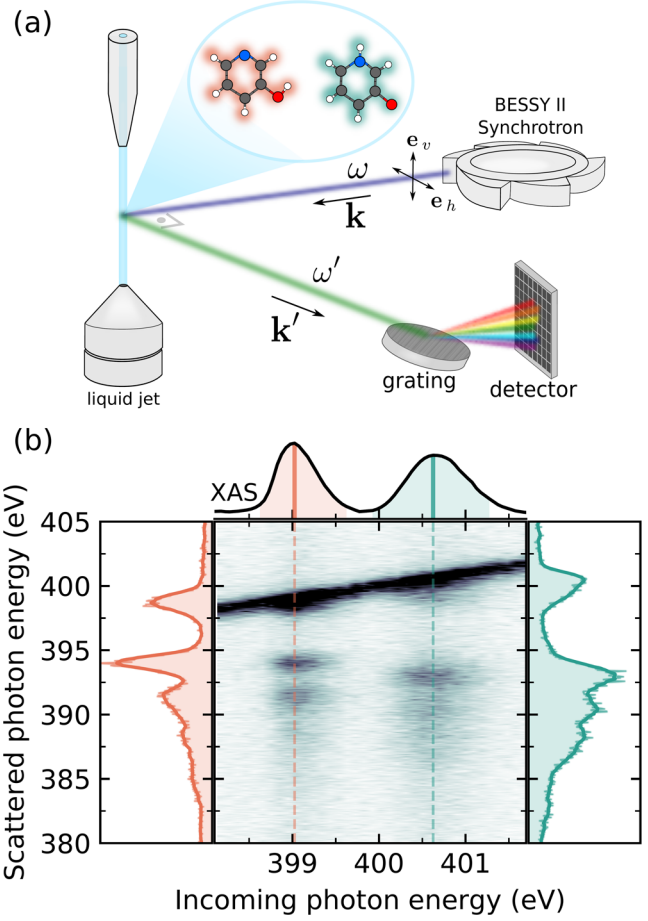

Figure 2. Experimental framework and 2D RIXS map of the tautomeric mixture. (a) Schematic of the experimental framework. (b) Measured RIXS map of aqueous 3-hydroxypyridine. On top, the X-ray absorption spectrum showing the separated resonances of each tautomer is shown. The individual spectrum of the enol is shown vertically on the left (399.0 eV excitation energy), and the individual spectrum of the keto (400.6 eV excitation energy) is shown vertically on the right.

https://doi.org/10.1021/acs.jpclett.1c03453
J. Phys. Chem. Lett. 2022, 13, 2459−2466

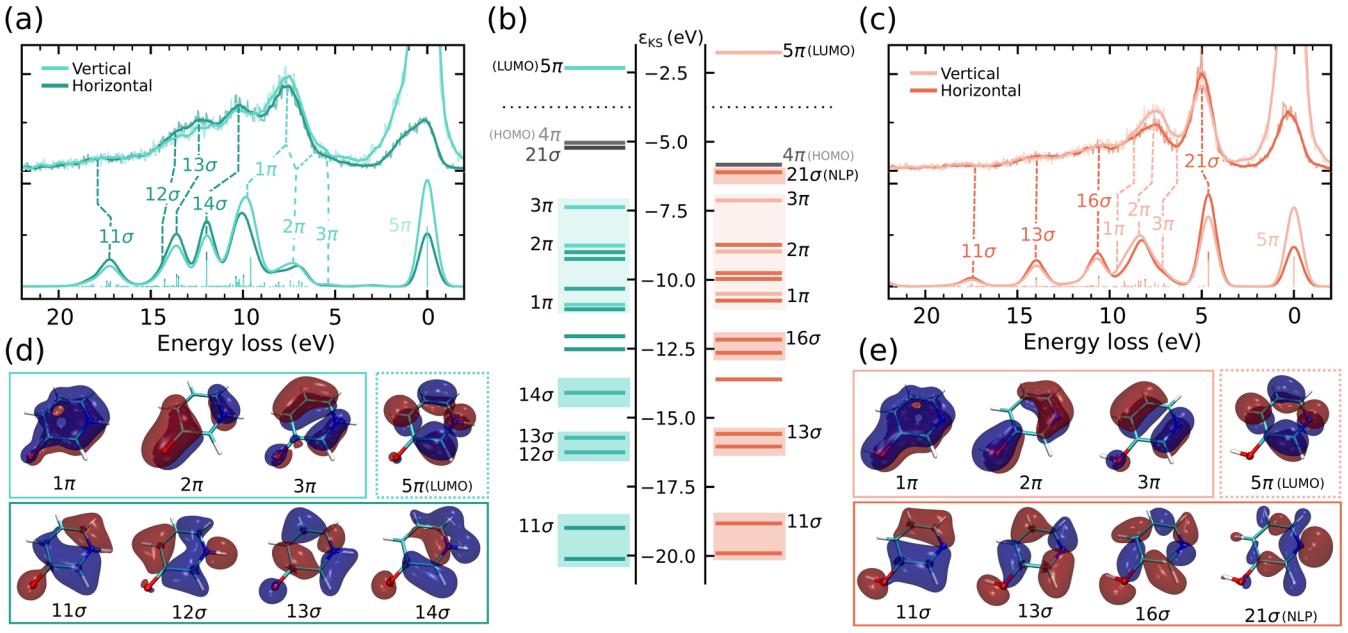

Figure 3. Scattering anisotropy and state assignment of the RIXS spectra of individual tautomers. Experimental and theoretical RIXS spectra of the (a) keto and (c) enol forms of 3-hydroxypyridine for both vertically and horizontally polarized excitation. (b) Kohn−Sham orbital-energy diagram highlighting significant orbitals. Relevant orbitals, grouped according to π and σ symmetry, used for assigning the RIXS spectra of the (d) keto and (e) enol forms.

From the 2D RIXS map, it can be clearly seen that we have well-defined regions associated with each tautomer. On the top axis of the map, we see the X-ray absorption spectrum showing the two π^* resonances, where the energetically lower one is associated with the enol species and the higher one is associated with the keto species. Since the absorption and emission steps are coupled in RIXS, the same selectivity holds for the scattered photons. It should be noted that such differentiation between species would be absent for other core-level methods, e.g., nonresonant X-ray emission or photoelectron spectroscopy. The resonant emission spectra for each of the tautomers are vertically plotted on the sides of the 2D map in Figure 2b. These spectra contain information on transitions between occupied molecular orbitals and the LUMO in the energy range up to 20 eV.

We elucidate the electronic differences introduced by the proton transfer connecting both species based on the recorded spectra of each tautomer. The first step is to assign the detected transitions in the spectra to electronic final states reached in the RIXS process. We do so on the basis of two tools: the scattering anisotropy of the RIXS process and time-dependent density functional theory calculations within the restricted subspace approximation[19] (RSA-TD-DFT). The inherent anisotropy of RIXS[20] allows the determination of the symmetry of the states present in the spectrum. Considering our experiment, excitation from a 1s orbital into an orbital of π symmetry with a vertically polarized photon leads to enhanced emission intensity from occupied π orbitals. The opposite is true for horizontally polarized excitation, where emission from σ orbitals is enhanced. This allows to assign regions of the RIXS spectrum associated with the π and σ bonding manifolds in a robust way. The experimental and theoretical RIXS spectra for horizontally and vertically polarized X-ray excitation are shown in Figure 3a,c for each tautomer.

The most prominent difference seen at the N K-edge RIXS spectra of the tautomers is the presence of the intense nitrogen lone-pair (21σ) peak at around 5 eV energy loss for the enol tautomer as seen in Figure 3c. This feature is absent in the spectrum of the keto species (Figure 3a) because in this case the corresponding orbital rehybridizes and binds covalently to the hydrogen 1s orbital to form the NH bond, which leads to a stabilization of the σ orbitals. This stabilization is consistent with the fact that 3HP is a weak acid (pK_a = 8.3[21]) with a strong N−H bond. Such an unambiguous signature of the lone-pair orbital has also been observed for deprotonated heterocycles.[10,22−24]

The position of the proton induces additional effects on the electronic structure of each tautomer, beyond the replacement of a lone pair by a N−H bond. More precisely, strong polarization of the occupied orbitals of each tautomer takes place. In general terms, the molecular orbitals in the keto form are polarized toward the nitrogen site, and in the enol form the orbitals are biased toward the oxygen atom. This is a reflection of the intuitive notion that the protonation of a given atom increases its ability to accommodate electron density.

Such polarization effects are very evident considering the π manifold of each system, in the energy loss range of 6−10 eV. Specifically, the fully bonding 1π orbital of each system (Figure 3d,e) shows a clear inversion of polarity between the nitrogen to oxygen atoms. This polarization is directly seen in the RIXS spectra (Figure 3a,c), where the keto species displays an intense peak associated with the 1π orbital and the intensity of the same orbital is much smaller in the enolic form, in which the 2π orbital carries the most intensity in the π manifold detected in the spectrum.

By analyzing the energy loss features beyond 10 eV, we identify transitions associated with the σ-bonding manifold, as also evidenced by the scattering anisotropy in both experiment and theory. For the keto form, four features that are associated with the delocalized ring orbitals, with a significant

https://doi.org/10.1021/acs.jpclett.1c03453
J. Phys. Chem. Lett. 2022, 13, 2459−2466

contribution from the N−H moiety, can be distinguished in this region: orbitals 14σ, 13σ, and 12σ in the region below 15 eV loss (Figure 3a,d). In the range between 15 and 20 eV, a weaker feature associated with the deep-lying 11σ orbital can be identified. Focusing now on the enol, we observe a considerably weaker intensity associated with the bonding σ peaks. This is a further indication of the polarization of these orbitals toward the O−H moiety and away from the nitrogen atom. Here, transitions from the 16σ and 13σ orbitals are detected in the 10−15 eV range (Figure 3c,e). Analogous to the spectrum of the keto, a weaker feature associated with the 11σ orbital is seen in the 15−20 eV energy loss range.

Finally, the role of the solvent in the equilibrium constant and in the electronic structure of each tautomer remains to be addressed. The general class of hydroxypyridines exhibits an inversion of the tautomeric equilibrium when substituting an apolar solvent for a polar one.[13,25,26] To further elucidate the role of the solvent, we performed QM/MM molecular dynamics simulations. Each tautomeric form of 3HP interacts strongly with the water molecules of the solvent via hydrogen bonds, leading to manifold configurations explored by each tautomer within its potential energy basin. Vibrational motion, both thermal- and X-ray-induced,[27] also plays a role in the formation of the spectrum. These aspects are not easily separable in the experimental data, so we need to investigate how each mechanism affects the peak positions, line shapes, and intensity ratios in the spectra.

Starting with the XAS, Figure 4 compares the effect of the core−hole lifetime broadening, the vibronic substructure, and

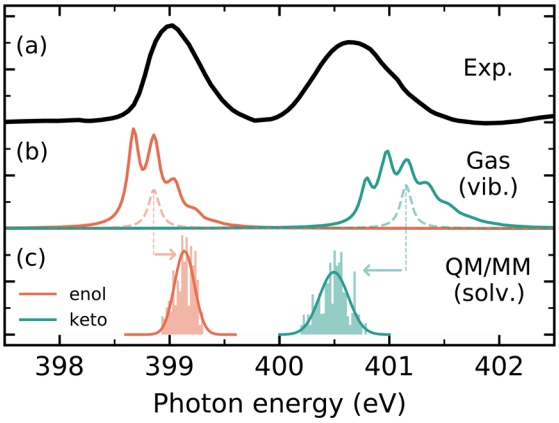

Figure 4. Effect of vibrational motion and solvation on the XAS spectral line shape. (a) Experimental XAS spectrum. (b) Calculated Franck−Condon profiles, in the gas phase, for each tautomer. The dashed lines show the absorption resonances including only the core−hole lifetime broadening (Γ_N = 0.12 eV, fwhm). (c) Calculated histograms of transition energies, weighted by their respective absorption intensities, sampled from the QM/MM MD simulations. From this analysis, we extract a tautomeric constant of K_T = 1.08.

the impact of solvation and thermal vibrations on the peak width and position. As can be seen, the width of the XAS resonances is dominated by the Franck−Condon progression of the modes active upon core excitation. However, no fine structure is seen in the experimental data because of the effect of solvation, which induces an additional broadening of the lines. We determined the solvation broadenings to be 0.21 eV (enol) and 0.31 eV (keto) from the histograms of transition energies, weighted by the absorption intensities, as shown in Figure 4c. In contrast, the vibrational broadenings (including the core−hole lifetime broadening) are estimated to be 0.96 eV (enol) and 1.10 eV (keto). Broadenings are given as full-width at half-maximum values. Using the computed line shapes, we extracted the tautomerization constant of 3HP from the ratio of the XAS peaks to be K_T = 1.08 ± 0.02 (Supporting Information), which is in good agreement with the values of Metzler and Snell[12] (K_T = 1.17), Sánchez-Ruiz et al.[25] (K_T = 1.10), and Llor and Asensio[26] (K_T = 1.06).

In our case, the tautomers are in chemical equilibrium. Hence, we observe a signal arising from the statistical distribution of proton positions around the potential energy basin minimum of each system as a consequence of the fluctuations of the hydrogen bond network around the nitrogen and oxygen sites. In cases of photoinduced tautomerism, the molecular vibrations can be mapped in real time through the oscillation of the position of the X-ray absorption lines, as demonstrated by Loe et al.[28]

Although the XAS lines are only modestly broadened by solvation, they are substantially shifted from the gas-phase resonance positions.[15] The shift is inverse for the two tautomers; namely, a blue shift is seen for the enol form, and a red shift is seen for the keto form. This indicates that hydrogen bonding reduces the electron density at the nitrogen site for the enol and increases it for the keto form. However, XAS is only an indirect measure of this effect since we probe unoccupied states. Hence, by turning to the RIXS transitions we may disentangle the origins of the changes in electron density distribution induced by solute−solvent interactions with molecular orbital specificity.

We can begin to uncover the detailed effects of hydrogen bonding by looking at the solvent distribution density plots in Figure 5a,b. As expected, an inversion of polarity in the solvation shell of each tautomer at the nitrogen site takes place. Moreover, it can be seen that solvation at the oxo site of the keto form is largely enhanced when compared to the hydroxyl group in the enol tautomer. This helps to explain the drastic stabilization of the keto form of the pyridones in aqueous solution.[13,15]

To clearly identify the effect of hydrogen bonding on the spectral observables, we calculated average RIXS spectra for each tautomer based on sampled configurations from the QM/MM MD trajectory. The spectra are shown in Figure 5c,d, where they are also compared to calculations in the gas phase. To link the observed changes in peak positions and intensity ratios seen in the theoretical simulations to the experimental RIXS spectra, we analyzed the charge density difference plots considering an idealized solvated cluster for each tautomer based on the microsolvation structures derived from the MD. The plots are shown in Figure 5e,f.

For the keto, σ density increases at the nitrogen while it decreases at the hydrogen. This is caused by the donated hydrogen bond to the water molecule, which increases the polarity of the N−H bond by decreasing the electron density at the hydrogen. In contrast, π-electron density is lost at the nitrogen site while it is accumulated at the C=O bond (Figure 5e). This solvent-induced orbital polarization is nicely reflected in the spectral simulations, which show that the relative intensity between the peaks of the π manifold and the σ manifold is reduced when comparing the gas phase and the explicitly solvated spectra in Figure 5c. The intensity difference is also accompanied by a 0.38 eV red shift of the π peak with respect to the gas phase.

https://doi.org/10.1021/acs.jpclett.1c03453
J. Phys. Chem. Lett. 2022, 13, 2459−2466

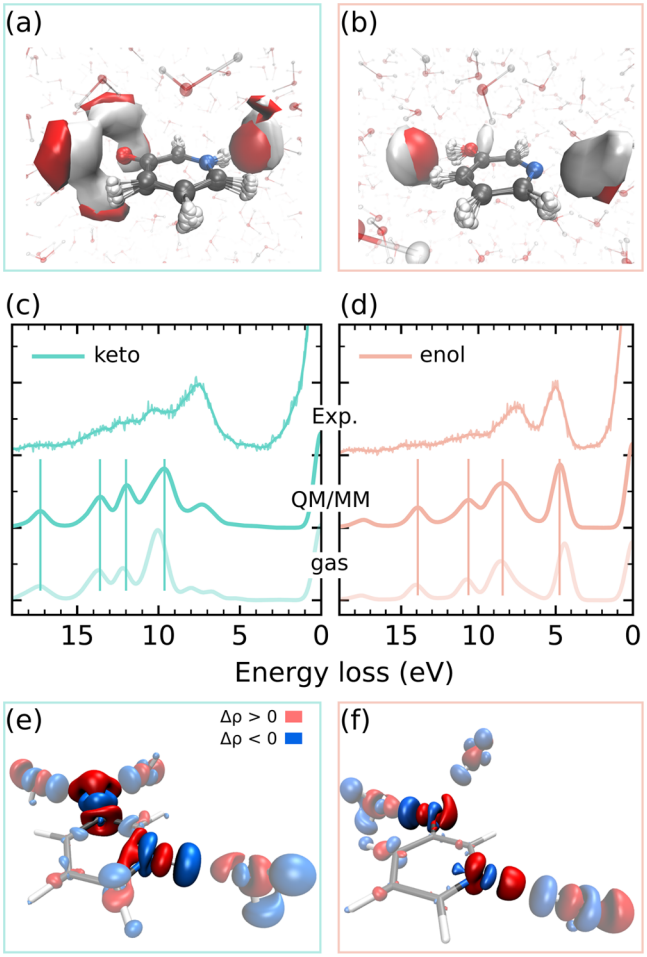

Figure 5. Hydrogen bonding effects on orbital polarization seen in the RIXS spectra. Solvent oxygen (red) and hydrogen (gray) mass-density distributions along with solute geometric distortions sampled from the QM/MM MD simulatons for the (a) keto and (b) enol tautomers. (c, d) Comparison between experiment and theoretical RIXS spectra, for vertically polarized excitation, computed from sampled snapshots from the MD as well as for the molecules in the gas phase. Electron density difference ($\Delta\rho$) for an idealized solvated cluster with respect to the molecule in vacuum for the (e) keto and (f) enol tautomers.

For the enol, we observe opposite trends. Specifically, a decrease in σ density at the nitrogen takes place as a result of the accepted hydrogen bond from a water molecule (Figure 5f). Synergetically, an increase in the π density occurs. Moreover, the solvation at the oxygen site creates a much less pronounced electron density reorganization in the enol tautomer than in the keto form. The shifts in electron density in the π and σ manifolds are also well captured in the RIXS spectra in Figure 5d, where we see an increase in the π peak with respect to the nitrogen lone-pair peak. We also see a 0.30 eV blue shift of the lone-pair peak with respect to the gas phase.

Molecular polarity and tautomerism are inextricably linked, as pointed out very early on by Lewis.[29] Polar chemical bonds result from the imbalance in the capacity of different atoms to attract the electrons in the molecule to their vicinity. The very fundamental reason for the existence of multiple tautomeric species of a given chemical compound stems from the shifts in polarity in the molecule, directly affecting their relative thermodynamic stability. This is further evidenced by the extreme influence of solvent polarity on tautomeric equilibria. Hence, the ability to experimentally dissect molecular polarity in terms of the concept of molecular orbitals is extremely powerful.

The example case of 3HP demonstrates how a technique capable of separating the overlapping spectral response of the tautomers yields new insights into electronic structure changes and orbital rehybridization introduced by the change in proton position. The association of RIXS intensities with the amplitude of bonding orbitals at a given elemental site is an inherent feature of X-ray spectroscopy in which a projected density of states is probed. Such a projection of molecular orbitals on atomic sites, by element-specific X-ray excitation, has been used, for instance, to quantify covalent interactions in transition-metal complexes.[30,31] In the specific case discussed here (the projection of the orbitals on the nitrogen site, which is one of the proton center sites), we are able to experimentally derive the change in electron density upon tautomerization and solvation.

The ability to assess the nitrogen 2p character of the bonding orbitals combined with the symmetry assignment provided by the scattering anisotropy enabled several interesting insights to be extracted. Notably, the lowest bonding π orbital is fully delocalized in both tautomers and is heavily biased to the nitrogen in the keto form and biased toward the oxygen in the enol form. A similar trend is seen for the σ-bonding orbitals, and the RIXS intensity of such states is higher for the keto form, indicating large amplitude at the nitrogen. They are, however, weaker in the enol form, indicating polarity toward the oxygen. Such an observation is consistent with the fact that the enol form is dominant in the gas phase because electron density accumulates at the more electronegative oxygen atom. This inherent picture is distorted once hydrogen bonding is accounted for. In this case, the considerably stronger interactions with the keto form lead to significant rehybridization at the nitrogen site, whereas the enol form is only modestly affected.

The effects discussed above have been only indirectly derived[1] or theoretically discussed.[32−35] The comprehensive review of Raczyńska et al.[1] extensively highlights the link between electron delocalization and polarization and the position of the tautomeric equilibrium. Notably, Sato et al.[34] discussed the concept of "electronic structure distortion" by solvation to explain the inversion of the tautomeric equilibrium in 2-pyridone when going from the gas phase to an aqueous solution. In that study, it was found by energy decomposition that the stabilization of the ketone is due to strong rehybridization of the orbitals at the hydrogen bonding sites. Our analysis for the 3HP isomer supports their notion with the added sensitivity of being able to experimentally disentangle the σ- and π-bonding manifolds of each system. Here, it becomes clear that future studies focusing on an experimental comparison of the same equilibrium in gas-phase apolar solvents and polar solvents will be able to track the electronic changes induced by the medium.

Generally, the large chemical shift of the XAS associated with proton transfer provides great selectivity in the RIXS spectra of prototropic tautomeric mixtures. Hence, we expect applicability to a wide range of systems, beyond the showcase of 3HP. Nevertheless, it should be noted that difficulties can arise on a system-specific basis, such as in the case where XAS resonances overlap, either completely or partially. In the less

https://doi.org/10.1021/acs.jpclett.1c03453
J. Phys. Chem. Lett. 2022, 13, 2459−2466

likely case of complete overlap, happening when the different tautomers exhibit chemically equivalent sites, selectivity would be drastically reduced. Here, the RIXS signal of the individual species would also overlap, requiring decomposition schemes to be applied. In the more probable case of only partial overlap, the concept of excitation energy detuning can be used to alter the relative contribution of the underlying species to the total signal by exciting on the blue or red flanks of the absorption resonances, thereby enabling at least partial recovery of the selectivity. Alternatively, even if the resonances overlap at a given elemental edge, the use of complementary elemental edges[28] provides further options to target the individual tautomeric forms.

In conclusion, we have established resonant inelastic X-ray scattering as a technique to separate the overlapping electronic structure of tautomers in equilibrium. The large protonation shift associated with the proton transfer at the isomerization site leads to well-separated resonances that can be excited selectively. The resulting spectra on the energy loss scale contain information on excitations from the occupied manifold to the LUMO of each system, and the intensities of each band report on the atomic character of a given occupied orbital, in the case presented here, at the nitrogen site. The symmetry of the states could be experimentally determined via the scattering anisotropy. Combining the experimental results with QM/MM MD simulations and RSA-TD-DFT spectral calculations, we were able to asses the intrinsic orbital polarization of the occupied manifold of each tautomer as well as the additional polarization induced by hydrogen bonding. The experimental scheme described here can be expected to be applicable to a wide range of systems and could lead to deeper insights into how the orbital polarization introduced by the proton transfer and the interactions with the solvent determine the position of the equilibrium between tautomers.

EXPERIMENTAL METHODS

The experiments were carried out at the BESSY II synchrotron facility. The X-ray absorption measurements were carried out using the nmTransmission NEXAFS endstation[36] at the UE52-SGM,[37] and the X-ray absorption spectra have been originally published by Büchner et al.[15] The RIXS measurements were performed at the UE49-SGM[38] beamline using the EDAX[39] endstation. The 3-hydroxypyridine (3HP) sample was purchased from Sigma-Aldrich with a minimum purity of 95% and dissolved in deionized water to yield a 75 mM solution. The experimental RIXS endstation is discussed in detail by Kunnus et al.[39] In short, the sample was delivered to the experimental vacuum chamber using a round liquid jet system of 20−30 μm diameter. The solution was refreshed at a rate of 1.3 mL/min. It was excited using horizontally and vertically polarized synchrotron radiation at the nitrogen 1s absorption resonances of the two tautomers with a bandwidth of 0.2 eV. The scattered photons were dispersed with respect to their energy and detected at a 90° angle using a modified Scienta XES 350 Rowland-type spectrometer.

COMPUTATIONAL METHODS

All electronic structure calculations were carried out with the ORCA package.[40] The RIXS scattering amplitudes were computed within the RSA-TD-DFT method described by Vaz da Cruz et al.[19] Transition moments were computed on the basis of the linear response amplitudes[41] using the Multiwfn[42] program. Spectral calculations used the PBE exchange and correlation functional and the def2-TZVP(-f) basis set.[43]

To model the microsolvation of each tautomer, quantum mechanics/molecular mechanics molecular dynamics (QM/MM MD) simulations were performed. The simulations used the NAMD/ORCA interface[44] in which ORCA[40] was used to compute the quantum mechanical forces of the solute molecules and NAMD[45,46] was used for the time propagation of the classical water molecules. The quantum-mechanical region was composed of only the solute molecule, treated at the B3LYP/def2-TZVP(-f) level using the RIJCOSX approximation,[47] while the solvent molecules were modeled via the classical TIP3P force field. From the simulations, uncorrelated snapshots were taken for the analysis of the solvation via radial distribution functions and to compute the XAS and RIXS spectra. Further details are available in the Supporting Information.

ASSOCIATED CONTENT

Supporting Information

The Supporting Information is available free of charge at https://pubs.acs.org/doi/10.1021/acs.jpclett.1c03453.

Theoretical and computational details of the spectral calculations, benchmark of exchange-correlation functionals, details of the molecular dynamics simulations including hydrogen bond analysis and radial distribution functions, effects of explicit solvation, spectral line shape analysis, tautomeric constant extraction, and resonance structures of 3-hydroxypyridine (PDF)

AUTHOR INFORMATION

Corresponding Author

Vinícius Vaz da Cruz − *Helmholtz-Zentrum Berlin für Materialien und Energie GmbH, Institute for Methods and Instrumentation for Synchrotron Radiation Research, 12489 Berlin, Germany;* orcid.org/0000-0001-9696-2498; Email: vinicius.vaz_da_cruz@helmholtz-berlin.de

Authors

Robby Büchner − *Universität Potsdam, Institut für Physik und Astronomie, 14476 Potsdam, Germany;* orcid.org/0000-0001-7077-4640

Mattis Fondell − *Helmholtz-Zentrum Berlin für Materialien und Energie GmbH, Institute for Methods and Instrumentation for Synchrotron Radiation Research, 12489 Berlin, Germany*

Annette Pietzsch − *Helmholtz-Zentrum Berlin für Materialien und Energie GmbH, Institute for Methods and Instrumentation for Synchrotron Radiation Research, 12489 Berlin, Germany*

Sebastian Eckert − *Helmholtz-Zentrum Berlin für Materialien und Energie GmbH, Institute for Methods and Instrumentation for Synchrotron Radiation Research, 12489 Berlin, Germany;* orcid.org/0000-0002-1310-0735

Alexander Föhlisch − *Helmholtz-Zentrum Berlin für Materialien und Energie GmbH, Institute for Methods and Instrumentation for Synchrotron Radiation Research, 12489 Berlin, Germany*

Complete contact information is available at: https://pubs.acs.org/10.1021/acs.jpclett.1c03453

Notes

The authors declare no competing financial interest.

■ ACKNOWLEDGMENTS

We thank the Helmholtz-Zentrum Berlin for the allocation of synchrotron radiation beamtime. A.F. and R.B. acknowledge funding from ERC-ADG-2014 Advanced Investigator Grant no. 669531 EDAX under the Horizon 2020 EU Framework, Programme for Research and Innovation.

■ REFERENCES

(1) Raczyńska, E. D.; Kosińska, W.; Ośmiałowski, B.; Gawinecki, R. Tautomeric Equilibria in Relation to Pi-Electron Delocalization. *Chem. Rev.* **2005**, *105*, 3561−3612.
(2) Munowitz, M.; Bachovchin, W.; Herzfeld, J.; Dobson, C.; Griffin, R. Acid-Base and Tautomeric Equilibria in the Solid State: Nitrogen-15 NMR Spectroscopy of Histidine and Imidazole. *J. Am. Chem. Soc.* **1982**, *104*, 1192−1196.
(3) Li, S.; Hong, M. Protonation, Tautomerization, and Rotameric Structure of Histidine: A Comprehensive Study by Magic-Angle-Spinning Solid-State NMR. *J. Am. Chem. Soc.* **2011**, *133*, 1534−1544.
(4) Hansen, A. L.; Kay, L. E. Measurement of Histidine pKa Values and Tautomer Populations in Invisible Protein States. *Proc. Natl. Acad. Sci. U.S.A.* **2014**, *111*, E1705−E1712.
(5) Weinstein, H.; Chou, D.; Johnson, C. L.; Kang, S.; Green, J. P. Tautomerism and the Receptor Action of Histamine: A Mechanistic Model. *Mol. Pharmacol.* **1976**, *12*, 738−745.
(6) Antonov, L.; Nedeltcheva, D. Resolution of Overlapping UV-Vis Absorption Bands and Quantitative Analysis. *Chem. Soc. Rev.* **2000**, *29*, 217−227.
(7) Antonov, L. *Tautomerism: Methods and Theories*; John Wiley & Sons, 2013.
(8) Gel'mukhanov, F.; Odelius, M.; Polyutov, S. P.; Föhlisch, A.; Kimberg, V. Dynamics of Resonant X-ray and Auger Scattering. *Rev. Mod. Phys.* **2021**, *93*, 035001.
(9) Biasin, E.; Nascimento, D. R.; Poulter, B. I.; Abraham, B.; Kunnus, K.; Garcia-Esparza, A. T.; Nowak, S. H.; Kroll, T.; Schoenlein, R. W.; Alonso-Mori, R.; et al. Revealing the Bonding of Solvated Ru Complexes with Valence-to-Core Resonant Inelastic X-ray Scattering. *Chem. Sci.* **2021**, *12*, 3713−3725.
(10) Eckert, S.; Norell, J.; Miedema, P. S.; Beye, M.; Fondell, M.; Quevedo, W.; Kennedy, B.; Hantschmann, M.; Pietzsch, A.; Van Kuiken, B. E.; et al. Ultrafast Independent N-H and N-C Bond Deformation Investigated with Resonant Inelastic X-Ray Scattering. *Angew. Chem., Int. Ed.* **2017**, *56*, 6088−6092.
(11) Vaz da Cruz, V.; Gel'mukhanov, F.; Eckert, S.; Iannuzzi, M.; Ertan, E.; Pietzsch, A.; Couto, R. C.; Niskanen, J.; Fondell, M.; Dantz, M.; et al. Probing Hydrogen Bond Strength in Liquid Water by Resonant Inelastic X-ray Scattering. *Nat. Commun.* **2019**, *10*, 1013.
(12) Metzler, D. E.; Snell, E. E. Spectra and Ionization Constants of the Vitamin B6 Group and Related 3-Hydroxypyridine Derivatives. *J. Am. Chem. Soc.* **1955**, *77*, 2431−2437.
(13) Beak, P.; Fry, F. S.; Lee, J.; Steele, F. Equilibration Studies. Protomeric Equilibria of 2- and 4-Hydroxypyridines, 2- and 4-Hydroxypyrimidines, 2- and 4-Mercaptopyridines, and Structurally Related Compounds in the Gas Phase. *J. Am. Chem. Soc.* **1976**, *98*, 171−179.
(14) Beak, P. Energies and Alkylations of Tautomeric Heterocyclic Compounds: Old Problems-New Answers. *Acc. Chem. Res.* **1977**, *10*, 186−192.
(15) Büchner, R.; Fondell, M.; Mascarenhas, E. J.; Pietzsch, A.; Vaz da Cruz, V.; Föhlisch, A. How Hydrogen Bonding Amplifies Isomeric Differences in Pyridones toward Strong Changes in Acidity and Tautomerism. *J. Phys. Chem. B* **2021**, *125*, 2372−2379.
(16) Eckert, S.; Miedema, P.; Quevedo, W.; O'Cinneide, B.; Fondell, M.; Beye, M.; Pietzsch, A.; Ross, M.; Khalil, M.; Föhlisch, A. Molecular Structures and Protonation State of 2-Mercaptopyridine in Aqueous Solution. *Chem. Phys. Lett.* **2016**, *647*, 103−106.
(17) Nolting, D.; Aziz, E. F.; Ottosson, N.; Faubel, M.; Hertel, I. V.; Winter, B. pH-Induced Protonation of Lysine in Aqueous Solution Causes Chemical Shifts in X-ray Photoelectron Spectroscopy. *J. Am. Chem. Soc.* **2007**, *129*, 14068−14073.
(18) Ekimova, M.; Quevedo, W.; Szyc, Ł.; Iannuzzi, M.; Wernet, P.; Odelius, M.; Nibbering, E. T. J. Aqueous Solvation of Ammonia and Ammonium: Probing Hydrogen Bond Motifs with FT-IR and Soft X-ray Spectroscopy. *J. Am. Chem. Soc.* **2017**, *139*, 12773−12783.
(19) Vaz da Cruz, V.; Eckert, S.; Föhlisch, A. TD-DFT Simulations of K-edge Resonant Inelastic X-ray Scattering Within the Restricted Subspace Approximation. *Phys. Chem. Chem. Phys.* **2021**, *23*, 1835−1848.
(20) Gel'mukhanov, F.; Ågren, H. Resonant Inelastic X-ray Scattering with Symmetry-Selective Excitation. *Phys. Rev. A* **1994**, *49*, 4378−4389.
(21) Barlin, G. B.; Pfleiderer, W. Ionization Constants of Heterocyclic Substances. Part IX. Protonation of Aminopyridones and Aminopyrimidones. *J. Chem. Soc. B* **1971**, 1425−1432.
(22) Eckert, S.; Vaz da Cruz, V.; Ochmann, M.; von Ahnen, I.; Föhlisch, A.; Huse, N. Breaking the Symmetry of Pyrimidine: Solvent Effects and Core-Excited State Dynamics. *J. Phys. Chem. Lett.* **2021**, *12*, 8637−8643.
(23) Eckert, S.; Niskanen, J.; Jay, R. M.; Miedema, P. S.; Fondell, M.; Kennedy, B.; Quevedo, W.; Iannuzzi, M.; Föhlisch, A. Valence Orbitals and Local Bond Dynamics around N Atoms of Histidine under X-ray Irradiation. *Phys. Chem. Chem. Phys.* **2017**, *19*, 32091−32098.
(24) Meyer, F.; Blum, M.; Benkert, A.; Hauschild, D.; Jeyachandran, Y. L.; Wilks, R. G.; Yang, W.; Bär, M.; Reinert, F.; Heske, C.; et al. Site-Specific Electronic Structure of Imidazole and Imidazolium in Aqueous Solutions. *Phys. Chem. Chem. Phys.* **2018**, *20*, 8302−8310.
(25) Sánchez-Ruiz, J. M.; Llor, J.; Cortijo, M. Thermodynamic constants for tautomerism and ionization of pyridoxine and 3-Hydroxypyridine in water-dioxane. *J. Chem. Soc., Perkin Trans. 2* **1984**, 2047−2051.
(26) Llor, J.; Asensio, S. B. Thermodynamics of the Solution Equilibria of 3-Hydroxypyridine and Pyridoxine in Water-Dioxane Mixtures. *J. Sol. Chem.* **1995**, *24*, 1293−1305.
(27) Vaz da Cruz, V.; Ignatova, N.; Couto, R. C.; Fedotov, D. A.; Rehn, D. R.; Savchenko, V.; Norman, P.; Ågren, H.; Polyutov, S.; Niskanen, J.; et al. Nuclear Dynamics in Resonant Inelastic X-ray Scattering and X-ray Absorption of Methanol. *J. Chem. Phys.* **2019**, *150*, 234301.
(28) Loe, C. M.; Liekhus-Schmaltz, C.; Govind, N.; Khalil, M. Spectral Signatures of Ultrafast Excited-State Intramolecular Proton Transfer from Computational Multi-edge Transient X-ray Absorption Spectroscopy. *J. Phys. Chem. Lett.* **2021**, *12*, 9840−9847.
(29) Lewis, G. N. Valence and Tautomerism. *J. Am. Chem. Soc.* **1913**, *35*, 1448−1455.
(30) Kroll, T.; Baker, M. L.; Wilson, S. A.; Lundberg, M.; Juhin, A.; Arrio, M.-A.; Yan, J. J.; Gee, L. B.; Braun, A.; Weng, T.-C.; et al. Effect of 3d/4p Mixing on 1s2p Resonant Inelastic X-ray Scattering: Electronic Structure of Oxo-Bridged Iron Dimers. *J. Am. Chem. Soc.* **2021**, *143*, 4569−4584.
(31) Baker, M. L.; Mara, M. W.; Yan, J. J.; Hodgson, K. O.; Hedman, B.; Solomon, E. I. K- and L-edge X-ray Absorption Spectroscopy (XAS) and Resonant Inelastic X-ray Scattering (RIXS) Determination of Differential Orbital Covalency (DOC) of Transition Metal Sites. *Coord. Chem. Rev.* **2017**, *345*, 182−208.
(32) Wong, M. W.; Wiberg, K. B.; Frisch, M. J. Solvent Effects. 3. Tautomeric Equilibria of Formamide and 2-Pyridone in the Gas Phase and Solution: an ab initio SCRF Study. *J. Am. Chem. Soc.* **1992**, *114*, 1645−1652.
(33) Barone, V.; Adamo, C. Density Functional Study of Intrinsic and Environmental Effects in the Tautomeric Equilibrium of 2-Pyridone. *J. Phys. Chem.* **1995**, *99*, 15062−15068.
(34) Sato, H.; Hirata, F.; Sakaki, S. Distortion of Electronic Structure in Solvated Molecules: Tautomeric Equilibrium of 2-Pyridone and 2-

https://doi.org/10.1021/acs.jpclett.1c03453
J. Phys. Chem. Lett. 2022, 13, 2459−2466

Hydroxypridine in Water Studied by the RISM-SCF Method. *J. Phys. Chem. A* **2004**, *108*, 2097−2102.
(35) Zilberg, S.; Dick, B. Less Stable Tautomers Form Stronger Hydrogen Bonds: The Case of Water Complexes. *Phys. Chem. Chem. Phys.* **2017**, *19*, 25086−25094.
(36) Fondell, M.; Eckert, S.; Jay, R. M.; Weniger, C.; Quevedo, W.; Niskanen, J.; Kennedy, B.; Sorgenfrei, F.; Schick, D.; Giangrisostomi, E.; et al. Time-Resolved Soft X-ray Absorption Spectroscopy in Transmission Mode on Liquids at MHz Repetition Rates. *Struct. Dyn.* **2017**, *4*, 054902.
(37) Miedema, P. S.; Quevedo, W.; Fondell, M. The Variable Polarization Undulator Beamline UE52 SGM at BESSY II. *Journal of Large-Scale Research Facilities* **2016**, *2*, A27.
(38) Pietzsch, A.; Eisebitt, S. The UE49 SGM RICXS Beamline at BESSY II. *Journal of Large-Scale Research Facilities* **2016**, *2*, A54.
(39) Kunnus, K.; Rajkovic, I.; Schreck, S.; Quevedo, W.; Eckert, S.; Beye, M.; Suljoti, E.; Weniger, C.; Kalus, C.; Grübel, S.; et al. A Setup for Resonant Inelastic Soft X-ray Scattering on Liquids at Free Electron Laser Light Sources. *Rev. Sci. Instrum.* **2012**, *83*, 123109.
(40) Neese, F. The ORCA Program System. *Wiley Interdiscip. Rev. Comput. Mol. Sci.* **2012**, *2*, 73−78.
(41) Nascimento, D. R.; Biasin, E.; Poulter, B. I.; Khalil, M.; Sokaras, D.; Govind, N. Resonant Inelastic X-ray Scattering Calculations of Transition Metal Complexes Within a Simplified Time-Dependent Density Functional Theory Framework. *J. Chem. Theory Comput.* **2021**, *17*, 3031−3038.
(42) Lu, T.; Chen, F. Multiwfn: A Multifunctional Wavefunction Analyzer. *J. Comput. Chem.* **2012**, *33*, 580−592.
(43) Weigend, F.; Ahlrichs, R. Balanced Basis Sets of Split Valence, Triple Zeta Valence and Quadruple Zeta Valence Quality for H to Rn: Design and Assessment of Accuracy. *Phys. Chem. Chem. Phys.* **2005**, *7*, 3297−3305.
(44) Melo, M. C.; Bernardi, R. C.; Rudack, T.; Scheurer, M.; Riplinger, C.; Phillips, J. C.; Maia, J. D.; Rocha, G. B.; Ribeiro, J. V.; Stone, J. E.; et al. NAMD Goes Quantum: An Integrative Suite for Hybrid Simulations. *Nat. Methods* **2018**, *15*, 351−354.
(45) Phillips, J. C.; Hardy, D. J.; Maia, J. D. C.; Stone, J. E.; Ribeiro, J. V.; Bernardi, R. C.; Buch, R.; Fiorin, G.; Hénin, J.; Jiang, W.; et al. Scalable Molecular Dynamics on CPU and GPU Architectures with NAMD. *J. Chem. Phys.* **2020**, *153*, 044130.
(46) Ribeiro, J. V.; Bernardi, R. C.; Rudack, T.; Stone, J. E.; Phillips, J. C.; Freddolino, P. L.; Schulten, K. QwikMD − Integrative Molecular Dynamics Toolkit for Novices and Experts. *Sci. Rep.* **2016**, *6*, 26536.
(47) Neese, F.; Wennmohs, F.; Hansen, A.; Becker, U. Efficient, Approximate and Parallel Hartree-Fock and Hybrid DFT Calculations. A Chain-of-Spheres-Algorithm for the Hartree-Fock Exchange. *Chem. Phys.* **2009**, *356*, 98−109.

https://doi.org/10.1021/acs.jpclett.1c03453
J. Phys. Chem. Lett. 2022, 13, 2459−2466